Basalt fibre-reinforced high density polyethylene composite development using the twin screw extrusion process

Onuh Adole [a], Lorna Anguilano [a,*], Timothy Minton [a], James Campbell [a], Lavelle Sean [b], Samaras Valisios [c], Karnik Tarverdi [a]

[a] Brunel University London, United Kingdom
[b] SeaEnergies, United Kingdom
[c] Swansea University, United Kingdom

ARTICLE INFO

ABSTRACT

Offshore renewable energy can lead the way towards sustainable energy harvesting and support the achievement of the CO_2 reduction target by 2030. To achieve this goal it is necessary to decrease the manufacturing and deployment cost of the offshore devices. This paper focusses on the mechanical, chemical and microstructural assessment of a novel high density polyethylene (HDPE) reinforced with short basalt fibres for potential application as a hull material for wave energy devices. The choice of short fibres ensures the new composite can utilise existing low cost manufacturing methods for HDPE structures. In particular this study compares the properties of material with a recycled HDPE matrix with the properties of a material using a virgin HDPE matrix. The mechanical properties achieved by the novel composites exceed an improvement of ~300% in the properties of the monolithic polymer hence indicating the potential of this material, both for recycled and virgin HDPE. Furthermore, exploration in detail of the interaction fibres/matrix indicated the dynamic reaction between coupling agent and polymeric matrix showing the formation of molecular bonding perpendicular to the fibres, hence enhancing a 3D network that further increases the reinforcement abilities of the fibres.

1. Introduction

With an expected £5.4 billion cumulative benefit by 2040, tidal and wave energy devices are following the lead of offshore wind generation as a promising renewable energy system [1]. However, bottlenecks have been identified in the use of steel as the main material for the construction of the devices [2]. Steel increases the cost for deployment due to its weight and the number of potential failures because of corrosion and biofouling. While the use of polymeric materials such as high-density polyethylene is already ongoing in the piping and shipping industry, the impact and loads to be withstood by wave and tidal devices is such that large structures manufactured from HDPE would not be able to survive such applications. This paper focusses on the mechanical, chemical and microstructural assessment of a novel high density polyethylene (HDPE) reinforced with basalt fibres for potential application as a hull material for wave energy devices. The interest is in obtaining improved structural properties while retaining the resistance to corrosion and biofouling shown by HDPE.

With an ever-increasing need for composite materials in everyday applications due to their superior performance over monolithic matrices, the last two decades has witnessed a surge in the research and development of these composites, with polymer matrix composites (PMCs) being in the forefront. The benefits and applications of these composites are well documented of which PMCs have found the most success in upscaling for industrial applications [3–5].

The push in recent years has been the identification of suitable second-phase filler reinforcements for these monolithic matrices, which in combination produce a high performance composite. Ex-situ second filler phase reinforcements are usually fibrous or particulate in nature and are synthesised externally before being introduced into the matrix. The most common commercially available reinforcements used for PMC development that have been extensively investigated are carbon (graphite) fibres and fibreglass. While these reinforcements have their respective advantages, they are relatively cost intensive to synthesise [5].

The search for suitable and affordable reinforcements led to the

discovery of a naturally-occurring source: the most abundant bedrock on earth, igneous basalt rock. Basalt fibres (BF) were initially developed for military use; however after their declassification in the early 1990s they attracted attention for commercial applications [6]. Made from naturally-occurring volcanic rock, basalt fibre's main constituents are plagioclase ($NaAlSi_3O_8$–$CaAl_2Si_2O_8$) and pyroxene (general formula: XY $(SiAl)_2O_6$, where 'X' and 'Y' refer to ions such as Ca^{2+}, Mg^{2+}, Na^+, Fe^{2+} and more rarely Zn^{2+} and Mn^{+2}) [7]. As expected of a naturally-occurring rock, basalt can significantly vary in chemical composition depending on its deposit location, but typically comprise of SiO_2, Al_2O_3, Fe_2O_3, CaO, MgO, Na_2O, TiO_2 and K_2O in order of magnitude (as seen in Table 1) [7].

Basalt fibres possess qualities that are of interest for composite development including excellent corrosion, acid, alkali and wear resistance, good thermal properties, and high resistance to radiation and UV light [8]. Basalt fibres can be classified as situated between E-glass and carbon fibres in terms of mechanical properties. They outperform glass fibres with a higher elastic modulus (78–110 GPa) and tensile strength (2.8–4.8 GPa) although fall short of the performance of carbon fibres [8,9]. However, cheaper production costs make basalt fibres a cost-effective alternative to carbon fibres where the highest possible performance is not required; unlike carbon fibres and glass fibre reinforcements, the synthesis of basalt fibres is a simple, cost-effective, two-step process of melting and extrusion [8].

While there have been numerous studies [10–15] into the development of polymer-basalt composites, the main focus has been on fabricated basalt fibres weaves or sheets with a few investigating composites developed using the extrusion process. Bashtannik et al. [11] investigated the influence of extrusion processing parameters on the performance of the fabricated basalt-polypropylene composites. Arslan and Dogan [14] reported that fibre sizing significantly influences the performance of basalt fibre reinforced poly (butylene terephthalate) composites produced using a twin screw extruder. Using a single screw extruder for composite fabrication, an improved wear rate in basalt particles/low density poly-ethylene (LDPE) composite with increased basalt particle content was reported by Akinci et al. [15].

In this particular study, the development of a basalt fibre/HDPE composite was investigated using a co-rotating twin screw extruder. The mechanical properties, as well as physical properties of the fabricated composites are evaluated as a function of basalt fibre weight percent (wt %) content. Fibre sizing chemistry and its influence on composite performance is also analysed and discussed.

2. Material and methods

2.1. Materials

Two polymeric matrices were used for this study: primary high density polyethylene (PHDPE) and secondary high density polyethylene (SHDPE). The primary resin (HPA 020HD5) was a high molecular weight HDPE in the form of pellets manufactured by *ExxonMobil*. The resin has a density of 0.9 g/cm^3, high load melt index (190 °C/21.6 kg) of 9.0 g/10 min and vicat softening temperature of 126 °C. This high molecular weight resin was chosen because of its excellent balance of rigidity, environmental stress crack resistance (ESCR), and impact strength. Typical values of tensile modulus and yield strength are 1 GPa and 21 MPa respectively, based on ASTM D638 standards [16]. The SHDPE, equally in pellet form, was sourced from a local recycling facility and had a density of ~0.9 g/cm^3

Four basalt fibres types were used as reinforcement in this study and

were supplied by Basaltex Ltd, Base Mineral Technologies (BMT) LLC and Mafic Black Basalt Irl Ltd. All four fibres were of similar length (6 ± 2.00 mm) with an average diameter of 15 ± 3.00 μm. For the purpose of the article the fibres are anonymised.

2.2. Fibre characterisation

As-received fibres were analysed using Energy Dispersive X-Ray Spectroscopy (EDS) in a Scanning Electron Microscope (SEM) and Fourier-transform infrared spectroscopy (FTIR). Novitskii [17] reported that the mechanical properties of basalt fibres vary depending on their chemical compositions; taking this into consideration, the fibres were analysed and their chemical compositions quantified using EDS area analysis (see Table 2). Strands of the fibres were mounted in an epoxy resin with their cross section normal to the base of the mount. The epoxy puck was ground, polished and carbon coated for EDS analysis in the SEM.

Fibre sizing analysis was conducted using a PerkinElmer FTIR spectrometer in attenuated total reflection (ATR) mode. ~ 5 g of basalt fibres were placed in a furnace at 800 °C and held for 2 h to burn off the loosely-bound sizing components. The fibres were then washed in ethanol followed by distilled water and held in an oven at ~80 °C for 1 h. The background was taken using these degraded fibres after which analysis was conducted on their corresponding as-received samples. Analyses were performed within a wave number range of 4000–450 cm^{-1}.

2.3. Composite fabrication

Basalt fibres were introduced into the extruder using a twin screw volumetric feeder (Fig. 1) and evenly distributed and dispersed in the HDPE resin with the aid of a co-rotating twin-screw extruder. In order to limit fibre damage, 40 mm diameter screws (21:1 length to diameter ratio) were used to mechanically distribute and disperse the fibres within the matrix. The extruder had five barrel zones from material feeding point to extrusion nozzle. In order to limit heat degradation of fibre sizing, all barrel zones were monitored and maintained at 200 ± 10 °C, using k-type thermocouples. The screws were driven at a rotational speed of 80 RPM, continuous composite strands were extruded through a 4 mm die which was rapidly cooled in a water trough at a temperature of ~15 °C, after which they were pelletised. The pellets were then dried for ~12 h in an oven at 70 °C to drive off moisture from the composite material.

2.4. High load melt index (HLMI) tests

The HLMI of the composites were measured using a *Thermo HAAKE MeltFlow ST* melt flow indexing instrument following ISO 1133 standards (2.095 × 8 mm capillary die head). The barrel was charged with

Table 2
Chemical composition (wt %) of supplied basalt fibres using EDS area analysis (5- point average).

	SiO$_2$	Al$_2$O$_3$	Fe$_2$O$_3$	CaO	MgO	Na$_2$O	K$_2$O	TiO$_2$
A	54.2	18.5	10.0	8.8	4.1	2.5	1.5	0.5
B	53.6	18.2	10.6	9.5	3.8	2.4	1.5	0.5
C	53.3	18.5	10.4	9.2	3.9	2.3	1.5	0.5
D	54.3	18.4	10.0	9.3	3.7	2.4	1.5	0.5

Table 1
Chemical composition of typical basalt fibres.

SiO$_2$	Al$_2$O$_3$	Fe$_2$O$_3$	CaO	MgO	Na$_2$O	TiO$_2$	K$_2$O
42.0–56.0	14.0–18.0	10.0–12.0	7.0–9.0	4.0–9.5	2.3–3.8	1.1–2.6	1.0–2.5

composite material and pre-heated for 5 min at a temperature of 190 °C. Measurements were taken for a weight loading of 21.6 kg at regular cut time interval of 30 s after which samples were cooled and weighed.

2.5. Thermal analysis

Differential scanning calorimetry (DSC) analyses were conducted using a *TA Instrument* DSC Q2000 analyser. ~5 mg composite charges were placed in a Tzero aluminium pan and the temperature was ramped at 10 °C per min between 40 °C and 250 °C in air. Thermal gravimetric analyses (TGA) were performed using a *TA Instrument* SDT Q600 analyser. Samples were placed in an alumina pan and the temperature was ramped at 10 °C per min from ambient temperature to 650 °C in air.

2.6. Tensile specimen manufacture

Composite pellets were fed into a DEMAG D150-452 NC III K injection moulding machine to produce conventional, axisymmetric flat dog bone-shaped specimens 4 mm thick and 10 mm wide. Processing temperatures across all barrel zones were kept below 200 °C. Samples of monolithic HDPE were equally extruded, injection moulded and tested to provide us a reference value used as a base against which composite improvements or deteriorations are measured.

2.7. Tensile and flexural testing

Measurement of the composite's tensile properties was performed using a universal Instron 4505 testing rig with *Zwick* measurement control, fitted with a clip-on resistive extensometer. Data was processed and analysed using TestXpert II testing software, following ISO 527 test methods.

Flexural testing was performed in accordance with ISO 178A using a 2 kN load cell. All tests were conducted in ambient conditions.

2.8. Charpy testing

Impact test were conducted using a *Zwick/Roell* Charpy impact tester following ISO 179–1:2010 standards. Impacts were flatwise and normal to the plane of reinforcement. Specimens were unnotched, 80 mm in length, 10 mm and 4 mm in width and thickness respectively. The composites' estimated charpy impact strengths were calculated from the corrected energy obtained from experimentation.

2.9. Microstructural characterisation

Scanning electron microscopy was performed on extruded composite pellets, as well as the tensile fracture surfaces using a *Zeiss Supra* 35VP high resolution equipped with a field emission gun (FEG). Samples were gold-sputter coated for analysis.

3. Experimental results

3.1. Fibre characterisation

Results from the EDS quantitative analysis show that all 4 fibres have similar bulk chemical composition (See Table 2). Mechanical property testing of the various fibres was not performed due to fibre length constraints. Nevertheless, Novitskii [17,18] reported that basalt fibres' mechanical and physical properties are largely dependent on source rock composition. It can thus be assumed that the fibres used in this study possess similar mechanical properties.

Fig. 2 shows the absorbance spectra of two selected fibre surfaces, *Fibre C* and *D*. It is well known that most fibres used for PMCs are treated with a sizing during manufacture, usually consisting of a film former and organosilane, to improve the interface adhesion and composite performance. However, manufacturers engineer the sizing chemistry and structure for specific polymer systems which usually remains proprietary knowledge. Therefore, an FTIR investigation aimed at highlighting the functional group differences in all four fibres, was performed, as these differences play a significant role in interface reaction bonding [12].

Analysis of FTIR spectra in Fig. 2 shows that both fibres were not solely treated with silane coupling agents. While all fibre sizings appeared to contain more components than organosilanes, distinct bands were observed in *Fibre D* which were absent in all other fibres. The bands at around 3350 cm^{-1} (stretching in N–H/O–H bonded to C and Si), 2950-2900 cm^{-1} (stretching in C–H of CH, CH2 and CH3), 1750-1650 cm^{-1} (stretching in C=O in esters/carbonyl) and 845 cm^{-1} (stretching in C–O–C in oxirane) are characteristic of epoxy resins used as a film former known to enhance fibre processing and improve composite performance [19].

An evaluation of the interaction between the fibres and the matrix was performed using micro-FTIR mapping as seen in Fig. 3, specifically highlighting the characteristic bands identified in *Fibre D*. The selection was informed by the improved mechanical properties of *Fibre D* compared to other fibres, which will be presented in subsequent sections.

The evaluation of the potential interaction between the sizing composition and the matrix indicated that the bonds identified by the bands at 2900-3000 cm^{-1} and 3250-3450 cm^{-1} create a strong link between the fibre surface and the matrix. It is hypothesised that the link is due to the terminal CH_2 of the epoxy linking with the H atom of the HDPE to form a stronger CH_3 bonding perpendicular to the surface of the fibre as well as the terminal N of the epoxy linking with the C atoms of the HDPE. The double link formed between the epoxy fraction of the sizing of *Fibre D* identified by the areas of strong absorbance within the analysed bands could be responsible for the improved mechanical behaviour of the overall composite.
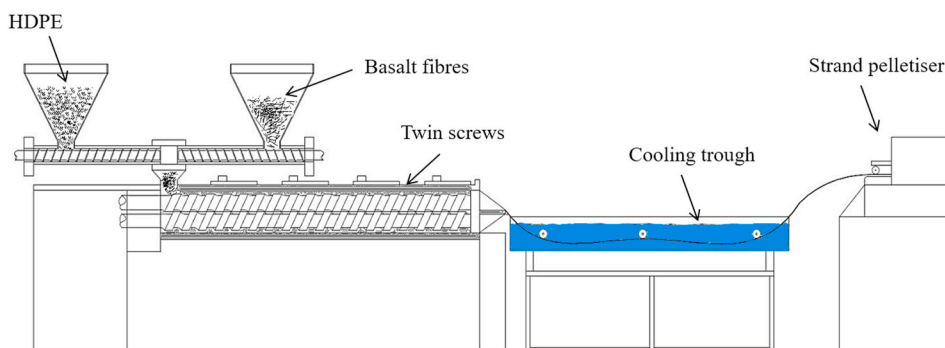

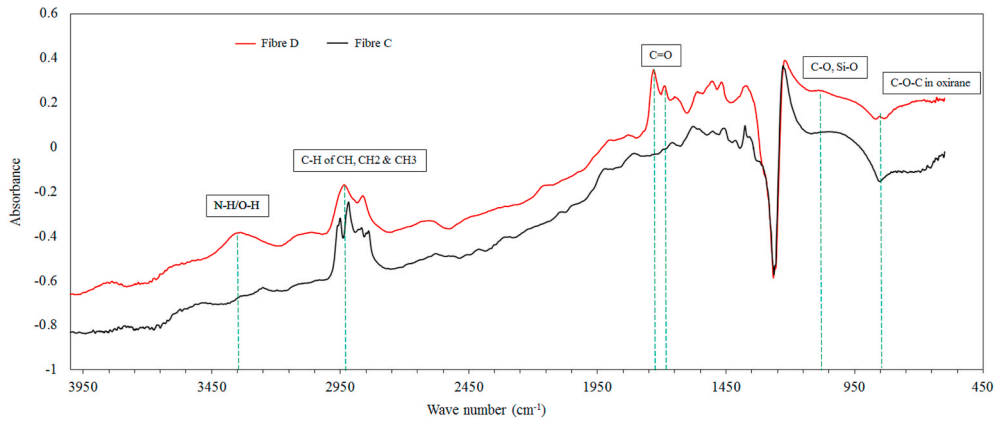**Fig. 1.** Schematic diagram of the twin screw extrusion process used to develop the composite.

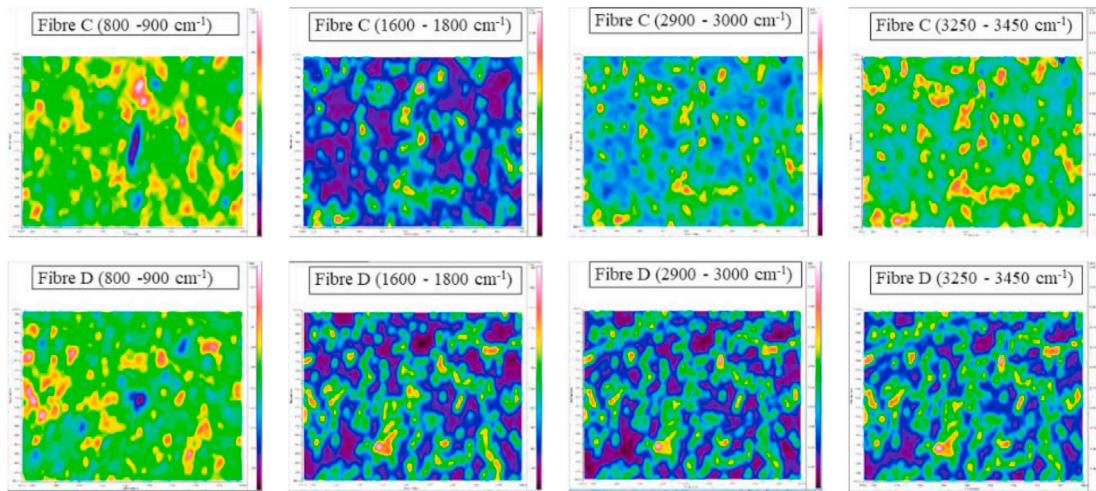**Fig. 2.** FTIR spectra of selected fibres (C and D) showing distinct peak variations.

Fig. 3. FTIR absorbance intensity map highlighting sizing-polymer interaction in selected composites (C and D).

3.2. Melt flow index

Fig. 4 shows the melt flow rates (MFR) of HDPE/basalt fibre composites. In order to better understand the MFR results, a basic ashing test was conducted to obtain the average length (0.67 ± 0.13 mm) of basalt fibres in the composite pellets before tests were conducted. As expected, there was a drop in the MFR of composites when compared to the monolithic matrices. A steady decrease was recorded in composites developed using SHDPE matrix with increasing fibre content. The low viscosity of the SHDPE matrix ensures that the fibres are given the freedom to align in the flow direction. However, not all fibres align leading to fibre entanglement which in turn restricts flow. This

entanglement is largely influenced by increasing fibre content. This is seen as the primary reason for the decrease in composite MFR.

On the other hand, composites developed using PHDPE had mixed results. *Fibre B* composites containing 10 wt% BF saw their MFR increase by ~240%. Even at 20 wt% addition, MFR of Fibre B composite remains higher than the monolithic matrix; increased MFR indicates lower viscosity which could be as a result of the breaking of polymer bonds as a direct result of fibre sizing-polymer interaction. *Fibre D* shows a constantly lower MFR in comparison with the reference and the other composites. However, at maximum basalt fibre addition, flow is restricted due to entanglement for all fibres.
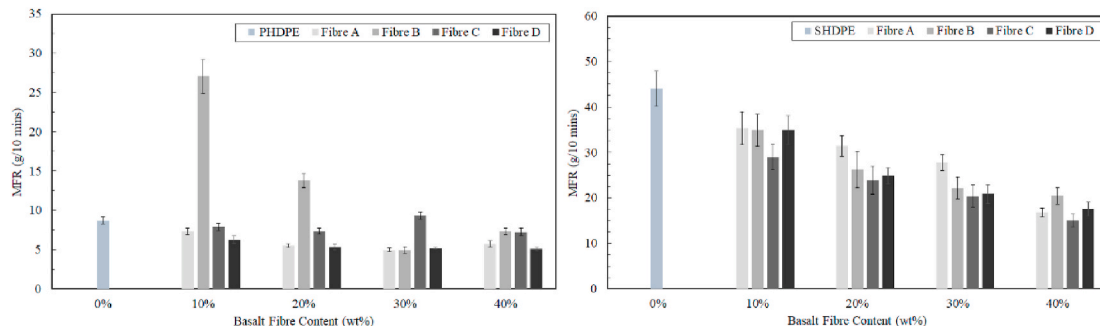

Fig. 4. High melt flow rate of composites as a function of increasing fibre wt%.

3.3. Thermal analysis results

3.3.1. TGA results

The thermogravimetric analysis results of the HDPE/BF composites are shown in Fig. 5. The TGA scans reveal that the twin-screw processing method is effective in the dispersion of the basalt fibres within the polymer matrix. The high thermal degradation range of the mineral-based basalt fibres (~800 °C) ensures there is no overlap of degradation temperatures. This provides a high degree of confidence in accurately assessing the effectiveness of this processing method. The TGA scans of a selected *Fibre D* composite as shown in Fig. 5 (a) indicates weight loss starting at ~260 °C for all samples. The monolithic PHDPE undergoes a steep weight loss at ~400 °C with complete degradation at ~450 °C; the composites' weight loss, on the other hand, is not as sharp with a complete degradation temperature range of 460–490 °C. While the difference is not significant, it indicates that addition of basalt fibres to the PHDPE offers the composite with a certain degree of thermal stability.

Fig. 5 (b) shows the TGA curves of composites developed with SHDPE. It can be seen that thermal degradation of monolithic SHDPE is similar to PHDPE. Degradation starts at ~260 °C, a sharp loss in weight percent at ~400 °C and complete degradation at ~450 °C. Upon addition of basalt fibres, even at 10 wt%, a significant shift in the thermal degradation is observed which starts at around 450 °C and complete degradation for all composites at around 500 °C. This again highlights the role of basalt fibres in the thermal stability of HDPE/BF composites. In light of this, it is important to note that improved thermal stability could be as a result of the beneficial sizing interaction with the polymer. Overall TGA analysis of composites developed using different fibre types showed improved thermal stability over monolithic matrices; however, the increases recorded were not as significant.

3.3.2. DSC results

The DSC thermograms of composites developed using *Fibre C* and *D* in PHDPE and SHDPE matrices are shown in Fig. 6. The graphs show a singular, well-defined maximum exothermic peak (T_{max}) for all samples, with both monolithic polymers recording exothermic peaks at ~117 °C corresponding to typical HDPE. The introduction of basalt fibres fillers into the PHDPE resulted in slight shifts in the exothermic peaks, although no trend was observed. SHDPE composites, on the other hand, showed a particular trend in the exothermic peak shifts. All composite peaks moved to the left of the monolithic SHDPE peak to lower temperatures.

3.4. Tensile and flexural properties

The mechanical properties of BF-reinforced PHDPE composites are shown in Fig. 7. Table 3 also summarises BF reinforced PHDPE as a function of fibre content. Unsurprisingly, there was a linear increase in the tensile and flexural moduli for all composites developed with increasing fibre content. *Fibre C* and *D* composites are highlighted as they lie on opposite ends in terms of performance. Overall results show

that composites developed using *Fibre D* as reinforcement outperform all other fibres. At 40 wt% fibre addition, *Fibre D* composites recorded a 411% and 492% increase in tensile and flexural moduli respectively; composites developed with *Fibre C* showed the smallest change of all 4 fibres with an increase of 283% and 321% respectively. Tensile modulus increased by 90% while an 80% increase in flexural modulus was obtained after adding only 10 wt% of *Fibre D*. For the strength of the composites, while an improvement was generally observed it was not as marked as the improvement in stiffness. Composites developed with *Fibre D* once again showed noticeable strength improvements over the other fibres. At 40 wt% of *Fibre D*, the composites showed an enhancement of 60% and 175% in tensile strength and flexural strength over the monolithic matrix. While there was an increase in the tensile and flexural strengths of composites developed using *Fibres A, B* and *D* as a function of increasing wt%, composites developed using *Fibre C* showed a steady decline in tensile strength (see Fig. 7(d)), although an enhancement was seen in flexural strength.

The mechanical properties of SHDPE reinforced with the 4 fibre types are summarised in Fig. 8.

It can be seen that the fibres provide reinforcing effects to the SHDPE matrix comparable to PHDPE. Addition of *Fibre D* to SHDPE yielded the best performing composite with an enhancement of 53% and 125% in tensile strength and flexural strength, at 40 wt% BF content. As was in the case of PHDPE, *Fibre C* had the least reinforcing effects on SHDPE, although the decline in tensile strength with increasing fibre content observed in HDPE was not observed; there was marginal enhancement of the tensile strength with increasing fibre content. The BF-SHDPE composites properties are summarised in Table 4.

In summary, the addition of even a small amount of fibre content (10 wt%) gave a significant increase in the material stiffness while not changing the strength. A higher fibre content (40 wt%) results in increased stiffness and strength. This was observed for both the PHDPE and SHDPE.

3.5. Impact strength

The impact strengths of the developed composites are depicted in Fig. 9 as determined from Charpy impact tests. For PHDPE composites, a general decline in the impact strength of the composites was observed with increasing fibre content. Interestingly, composites reinforced with *Fibre C* (overall lowest mechanical properties) performed significantly better than other composites. In the SHDPE matrix, *Fibre C* composite, once again, performed better than the other composites. This could be attributed to early fibre pull-out resulting in increased debond length. *Fibre D* composites (best average mechanical properties) in particular recorded the lowest impact strength values when used to reinforce both PHDPE and SHDPE matrices. The good fibre-matrix interfacial adhesion beneficial for tensile and flexural test could prove detrimental for this particular composite. Thomason and Vlug reported that for composite impact resistance strengthening, good interfacial adhesion must be accompanied by an increase in length [20].
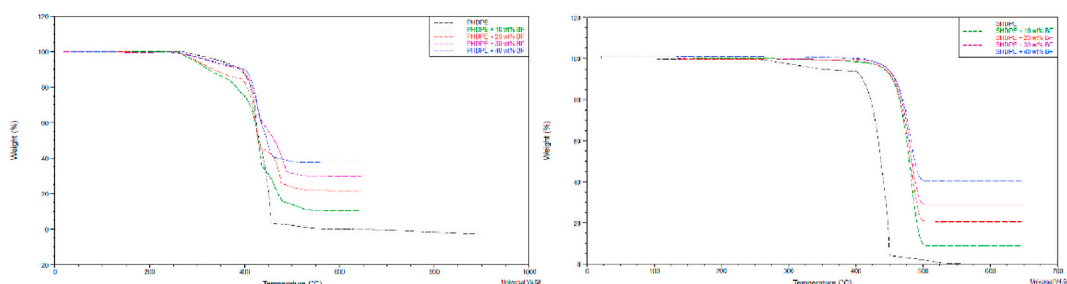

Fig. 5. Thermal degradation curves of selected composite developed using the twin-screw extrusion method.
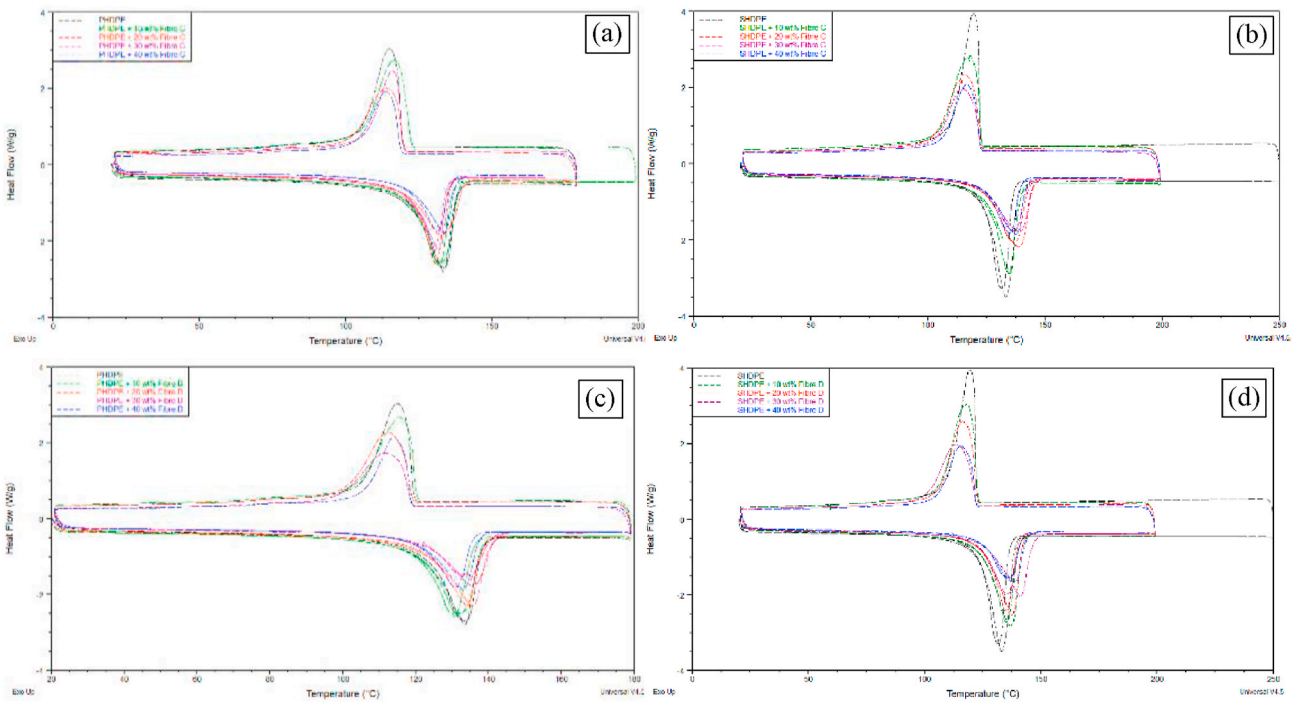
Fig. 6. DSC curves of *Fibre C* (a, b) and *Fibre D* (c, d) composites showing similar shifts in exothermic peaks.
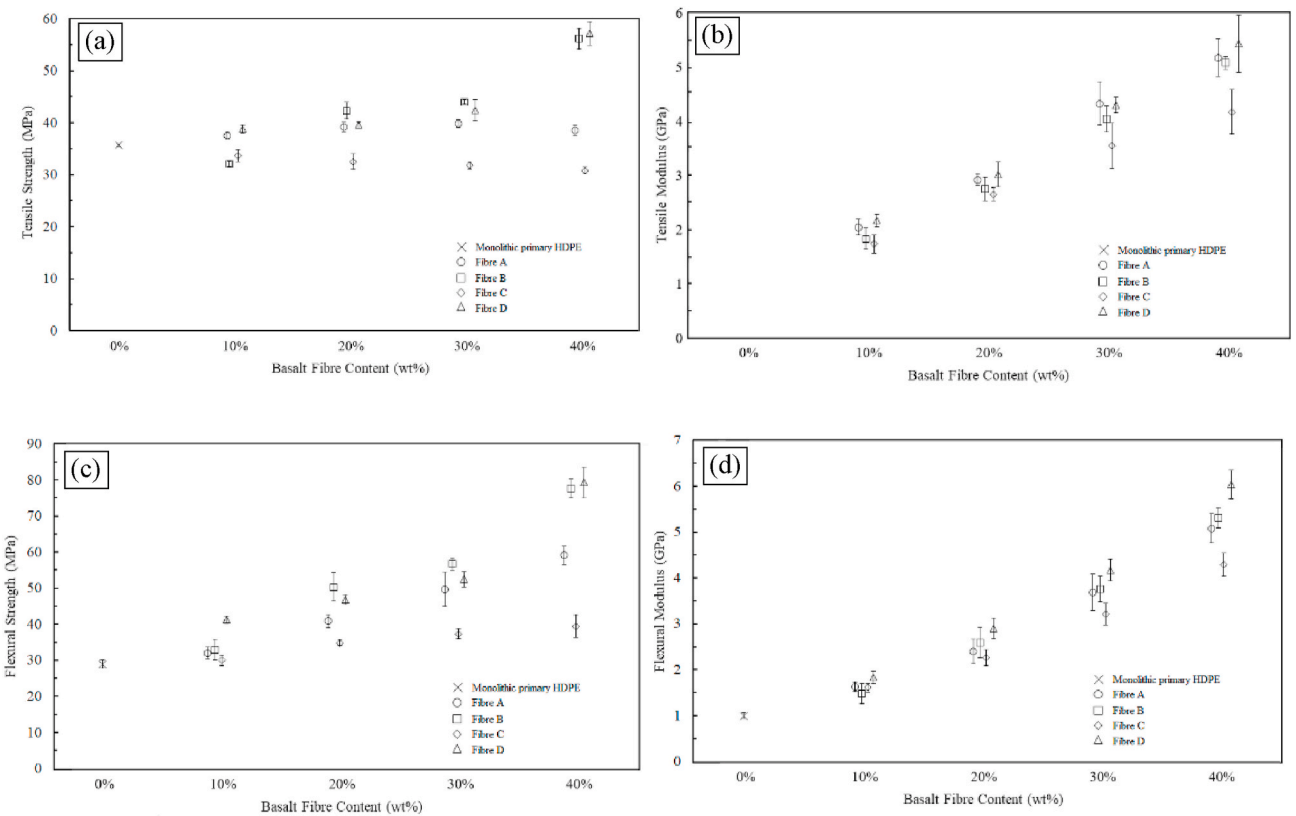

Fig. 7. Variations of (a) tensile strength, (b) tensile modulus, (c) flexural strength and (d) flexural modulus as a function of basalt fibre content in PHDPE/BF composite.

3.6. Microstructural characterisation

Fractographs of selected composites (*Fibres C* and *D*) after tensile testing were examined to understand the effect of sizing on adhesion between matrix and fibres. Fig. 10 shows the fracture surfaces of PHDPE composites containing 10 wt% basalt fibres at × 150 magnification. It can be seen that the plastic flow of the matrix with *Fibre D* is not as pronounced as that with *Fibre C* which suggests improved interfacial

Table 3

Mechanical properties of PHDPE/Basalt fibre composites (Strength in MPa, Moduli in GPa).

| Property	PHDPE	PHDPE/Fibre A				PHDPE/Fibre B				PHDPE/Fibre C				PHDPE/Fibre D			
	0 wt%	10 wt%	20 wt%	30 wt%	40 wt%	10 wt%	20 wt%	30 wt%	40 wt%	10 wt%	20 wt%	30 wt%	40 wt%	10 wt%	20 wt%	30 wt%	40 wt%
Tensile Strength	35.2	36.8	38.5	39.3	37.7	31.9	41.5	43.1	55.3	33.2	31.8	31.4	30.0	38.1	38.8	41.6	56.2
Tensile Modulus	1.1	2.0	2.8	4.3	5.1	1.8	2.7	4.0	5.0	1.7	2.6	3.5	4.1	2.1	3.0	4.2	5.5
Flexural Strength	28.8	32.1	40.7	49.7	59.4	32.9	50.2	56.6	77.6	30.1	34.7	37.0	39.8	41.2	46.6	52.4	79.2
Flexural Modulus	1.0	1.6	2.4	3.6	5.1	1.5	2.6	3.7	5.3	1.5	2.2	3.2	4.3	1.8	2.9	4.1	6.1
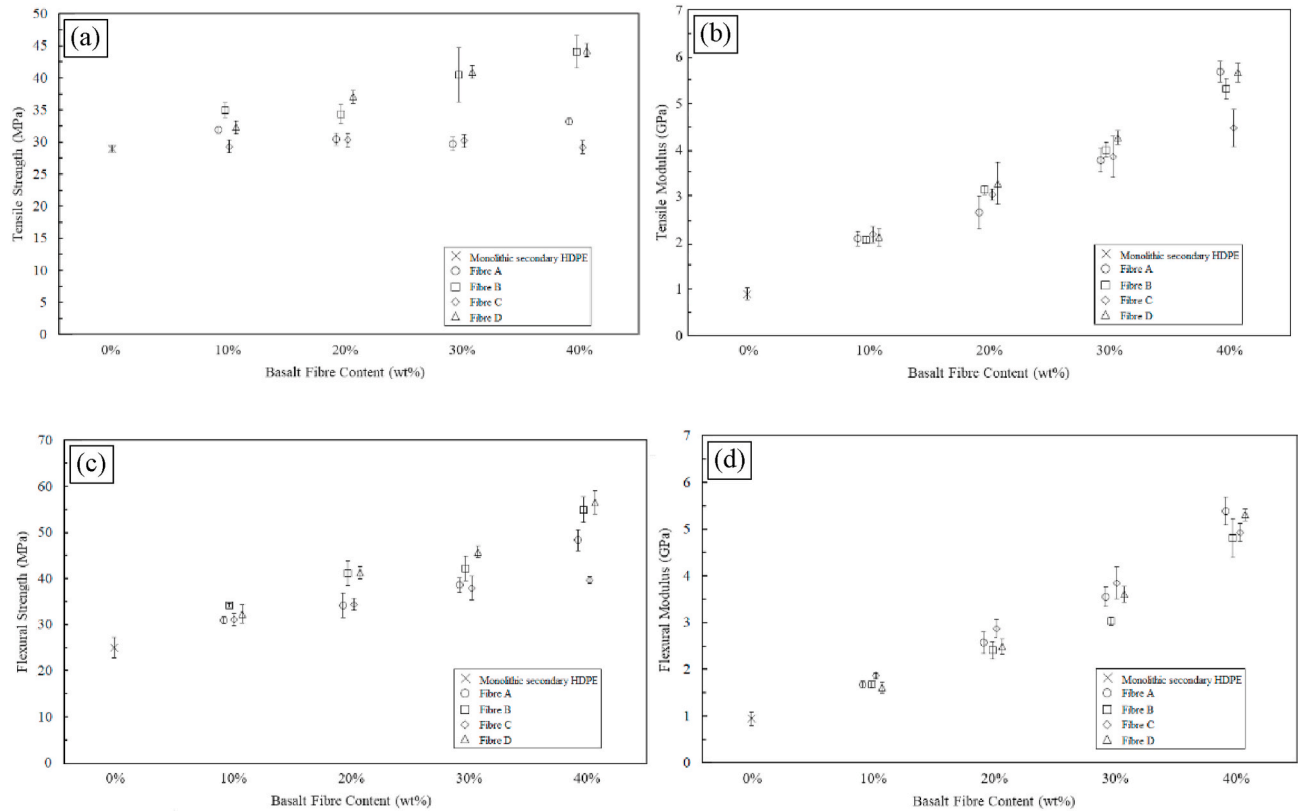
Fig. 8. Variations of (a) tensile strength, (b) tensile modulus, (c) flexural strength and (d) flexural modulus as a function of basalt fibre content in SHDPE/BF composite.

Table 4

Mechanical properties of SHDPE/Basalt fibre composites (Strength in MPa, Moduli in GPa).

Property	SHDPE	SHDPE/Fibre A				SHDPE/Fibre B				SHDPE/Fibre C				SHDPE/Fibre D			
	0 wt%	10 wt%	20 wt%	'30 wt%	40 wt%	10 wt%	20 wt%	30 wt%	40 wt%	10 wt%	20 wt%	30 wt%	40 wt%	10 wt%	20 wt%	30 wt%	40 wt%
Tensile Strength	29.1	31.5	30.4	29.8	33.2	34.8	34.2	40.7	43.9	29.5	30.2	30.4	29.1	32.2	37.1	40.6	44.4
Tensile Modulus	0.8	2.1	2.6	3.7	5.6	2.1	3.1	3.9	5.3	2.1	3.0	3.8	4.4	2.1	3.2	4.2	5.6
Flexural Strength	25.1	31.2	34.5	38.8	48.6	34.2	41.1	42.2	54.9	30.9	34.2	37.7	39.7	32.0	40.9	45.6	56.4
Flexural Modulus	0.9	1.6	2.5	3.5	5.3	1.7	2.4	3.0	4.8	1.8	2.8	3.8	4.9	1.5	2.4	3.6	5.2

adhesion between matrix and fibres. This good interfacial bonding in Fig. 10 (a) implies that the *Fibre D* sizing provided adequate bridging between matrix and fibres ensuring effective stress transfer; the equal fibre lengths and minimal plastic flow is seen as a result of uniform fibre failure. On the other hand, the increased plastic flow and long fibres seen on the fracture in Fig. 10 (b) indicates early debonding between *Fibre C* and matrix. This is indicative of ineffective adhesion provided by *Fibre C* sizings and the matrix which meant fracture occurred in the matrix as a
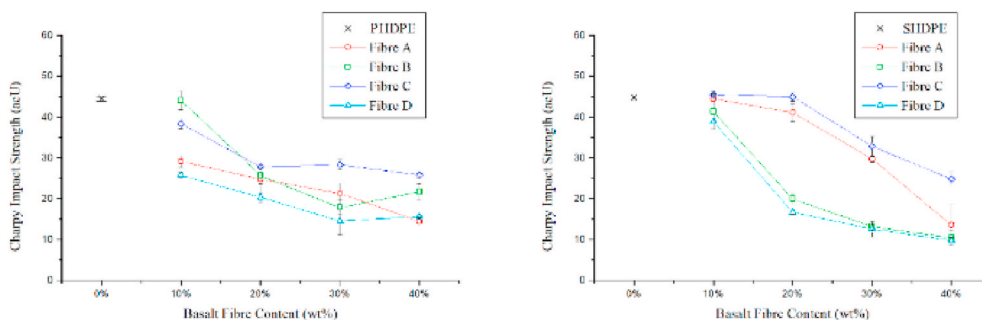
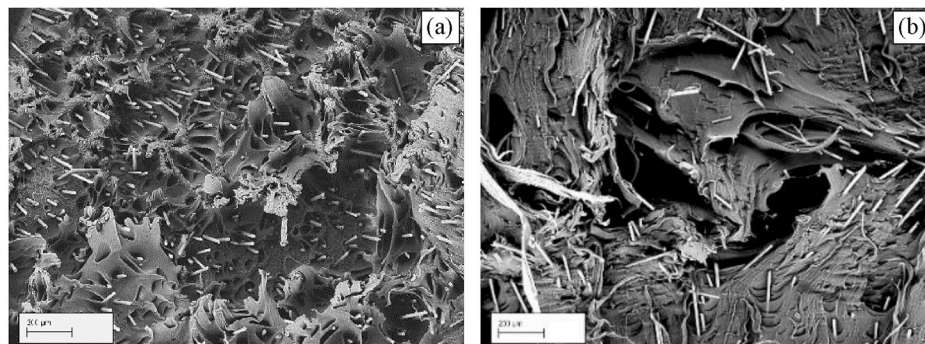**Fig. 9.** Charpy impact strengths of HDPE/BF composites with varying basalt fibre content.

Fig. 10. SEM micrographs of selected composite tensile specimens, (a) PHDPE/10 wt% *Fibre D*, (b) PHDPE/10 wt% *Fibre C*.

result of minimal load transfer to fibres.

The fibre-matrix interface for *Fibres C* and *D* of the selected composites were examined in more detail. Fig. 11 shows high magnification views of fibres exposed at the fracture surface of tensile specimens, with

Fig. 11 (a, b) showing that the *Fibre D* sizing promotes adhesion as indicated by the evolution of matrix around the fibres in a ripple-like effect. Examination of *Fibre D* interface under a higher magnification shows uniform distribution of bright resinous particulates on its surface,
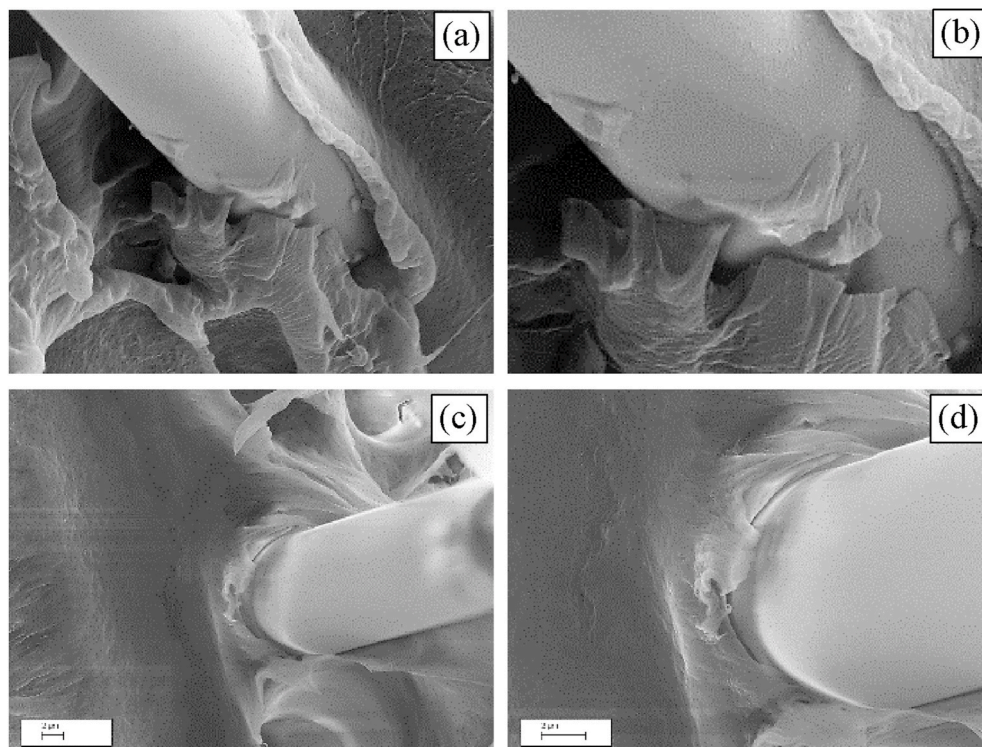

Fig. 11. High magnification SEM micrographs of fracture surfaces showing, (a–b) polymeric adhesion ripples in Fibre C composites, (c–d) debonding in Fibre D composites.

presumably the film former as seen in Fig. 11 (b). This is a result of the interaction between sizing and matrix material which provides the bridging and adhesion. On the other hand, these particles are absent on the surface of *Fibre C* (see Fig. 11 (c)). Also, the characteristic ripple-like bonding, usually promoted by epoxy resins, seen on *Fibre D* is not observed on the matrix/*Fibre C* interface. Fig. 11 (d) shows, instead, the matrix-fibre debonding occurs along the circumference of the *Fibre C* indicating the occurrence of weak adhesion. However, this weak bonding is not necessarily undesirable as it could account for the improved impact resistance performance of its composite as fracture energy is very much dependent on fracture mechanisms [21].

4. Conclusions

Mechanical, chemical and microstructural analysis of basalt fibre reinforced HDPE composites, comprising four different fibres (*A, B, C* and *D*) and two different HDPE matrices (primary and secondary), has been carried out.

The chemical evaluation of the interface fibre/matrix indicated that *Fibre D* had a unique spectra fingerprint indicating N–C and CH_3 bonding increase. It can be hypothesised that the CH_2 terminal bonding of the epoxy-rich coupling agent links with an H atom of the HDPE forming a stronger CH_3 molecular bonding. Furthermore, the terminal N atom of the resin also links with a C atom of the polymer creating a double interaction between fibre and matrix and strengthening adhesion. Overall up to 30 wt% fibre reinforcement is ideal as the low viscosity of SHDPE allows for fibre alignment, however, for concentration above this point fibre entanglement starts hindering the manufacturing process. For PHDPE, the effect is not linear as for SHDPE.

TGA results indicate that the composites' weight loss is not as sharp in comparison with the monolithic polymer, however the temperature range remains similar, even though a slightly higher temperature is observed for the composite, indicating an increased thermal stability. This is confirmed for both SHDPE and PHDPE and it could be a result of the beneficial sizing interaction with the polymer.

Evaluation of the mechanical properties indicate a linear increase in the tensile and flexural moduli for all composites developed increasing fibres content, however, composite developed with the use of *Fibre D* as reinforcement outperforms all other fibres. The impact strength, however, shows a dissimilar behaviour, in which composites reinforced with *Fibre C*, which has the lowest mechanical properties, performed significantly better than the other composites. This could be attributed to early fibre pull-out resulting in increased debond length. The good fibre-matrix interfacial adhesion beneficial for tensile and flexural test could prove detrimental for the composite developed with *Fibre D* as expressed by Thomason and Vlug [19] reporting that good interfacial adhesion must be accompanied by an increase in length.

The good interfacial bonding observed for *Fibre D* is linked to the development of the CH_3 and CN molecular bonding which implies that the *Fibre D* coupling agent provided adequate bridging between matrix and fibres, ensuring effective stress transfer. This is visible with the formation of ripple-like structure indicating full adhesion between the fibre and the matrix. This bonding seems responsible for the final significance highest performance of these fibres compared to the other ones. However, a weaker bonding, as shown by *Fibre C* might not be overall undesirable since it can account for improved impact resistance.

The results show that a short fibre Basalt-HDPE composite material, compatible with existing injection/extrusion HDPE manufacturing processes, with superior mechanical properties over monolithic HDPE can be manufactured. The final properties are significantly influenced by both the proportion of fibre present and the quality of the fibre-matrix interface. The addition of even a small proportion of basalt fibre to HDPE delivered a significant increase in material stiffness, a benefit shown for both primary and secondary HDPE material.

References

[1] Offshore Renewable Energy Catapult, Innovation Highlights 2018/19 [Online] Glasgow: ore.catapult.org.uk, 2019. Available at: https://s3-eu-west-1.amazonaws.com/media.neworE.catapult/app/uploads/2019/07/02130700/ORE-Catapult-Innovation-Highlights-2018-19.pdf. (Accessed 13 August 2019).

[2] R. James, W. Weng, Floating wind joint industry project phase I summary report. [Online] london: the carbon trust, Available at: https://www.carbontrust.com/media/675868/flw-jip-summaryreport-phase1.pdf, 2018. (Accessed 13 August 2019).

[3] B. Siswandi, W. Aryawan, High density polyethylene (HDPE) vessel of pompong as a fishing vessel for bengkalis fisherman, IPTEK Journal of Proceedings Series (2) (2017) 108, 0.

[4] G. Neşer, Polymer based composites in marine use: history and future trends, Procedia Eng. 194 (2017) 19–24.

[5] N. Gupta, M. Paramsothy, Erratum to: metal- and polymer-matrix composites: functional lightweight materials for high-performance structures, JOM (J. Occup. Med.) 67 (8) (2015), 1913-1913.

[6] V. Dhand, G. Mittal, K. Rhee, S. Park, D. Hui, A short review on basalt fiber reinforced polymer composites, Compos. B Eng. 73 (2015) 166–180.

[7] R. Subramanian, H. Austin, Silane coupling agents in basalt-reinforced polyester composites, Int. J. Adhesion Adhes. 1 (1) (1980) 50–54.

[8] V. Fiore, T. Scalici, G. Di Bella, A. Valenza, A review on basalt fibre and its composites, Compos. B Eng. 74 (2015) 74–94.

[9] J. Militky, V. Kovacic, Ultimate mechanical properties of basalt filaments, Textil. Res. J. 66 (4) (1996) 225–229.

[10] A. Paipetis, C. Galiotis, Effect of fibre sizing on the stress transfer efficiency in carbon/epoxy model composites, Compos. Appl. Sci. Manuf. 27 (9) (1996) 755–767.

[11] P. Bashtannik, V. Ovcharenko, Y. Boot, Effect of combined extrusion parameters on mechanical properties of basalt fiber-reinforced plastics based on polypropylene, Mech. Compos. Mater. 33 (6) (1997) 600–603.

[12] T. Deak, T. Czigany, P. Tamas, C. Nemeth, Enhancement of interfacial properties of basalt fiber reinforced nylon 6 matrix composites with silane coupling agents, Express Polym. Lett. 4 (10) (2010) 590–598.

[13] F. Gauvin, P. Cousin, M. Robert, Improvement of the interphase between basalt fibers and vinylester by nano-reinforced post-sizing, Fibers Polym. 16 (2) (2015) 434–442.

[14] C. Arslan, M. Dogan, The effects of silane coupling agents on the mechanical properties of basalt fiber reinforced poly(butylene terephthalate) composites, Compos. B Eng. 146 (2018) 145–154.

[15] A. Akinci, S. Yilmaz, U. Sen, Wear behavior of basalt filled low density polyethylene composites, Appl. Compos. Mater. 19 (3–4) (2011) 499–511.

[16] Exxonmobilchemical.ulprospector.com, 2019 [online] Available at: https://exxonmobilchemical.ulprospector.com/datasheet.aspx?I=58933&FMT=PDF&CULTURE=en-US&PS=PE&E=370558. (Accessed 25 October 2019).

[17] A. Novitskii, High-temperature heat-insulating materials based on fibers from basalt-type rock materials, Refract. Ind. Ceram. 45 (2) (2004) 144–146.

[18] A.G. Novitskii, V.V. Sudakov, An unwoven basalt-fiber material for the encasing of fibrous insulation: an alternative to glass cloth, Refractory Industrial Ceramics 45 (2004) 234–241.

[19] H.N. Petersen, Y. Kusano, P. Brondsted, K. Almdal, Preliminary characterisation of glass fibre sizing, Proceedings of the Risø International Symposium on Materials Science 34 (2013) 333–340.

[20] J. Thomason, M. Vlug, Influence of fibre length and concentration on the properties of glass fibre-reinforced polypropylene: 4. Impact properties, Compos. Appl. Sci. Manuf. 28 (3) (1997) 277–288.

[21] R. Muthuraj, M. Misra, F. Defersha, A. Mohanty, Influence of processing parameters on the impact strength of biocomposites: a statistical approach, Compos. Appl. Sci. Manuf. 83 (2016) 120–129.